

The Relationship Between Pulsatile Flow Impingement and Intraluminal Thrombus Deposition in Abdominal Aortic Aneurysms

RICHARD J. LOZOWY ¹, DAVID C. S. KUHN,¹ ANNIE A. DUCAS,² and APRIL J. BOYD²

¹Department of Mechanical Engineering, University of Manitoba, Winnipeg, MB, Canada; and ²Department of Surgery, University of Manitoba, Winnipeg, MB, Canada

(Received 24 August 2016; accepted 7 November 2016; published online 28 November 2016)

Associate Editors Tim McGloughlin and Ajit P. Yoganathan oversaw the review of this article.

Abstract—Direct numerical simulations were performed on four patient-specific abdominal aortic aneurysm (AAA) geometries and the resulting pulsatile blood flow dynamics were compared to aneurysm shape and correlated with intraluminal thrombus (ILT) deposition. For three of the cases, turbulent vortex structures impinged/sheared along the anterior wall and along the posterior wall a zone of recirculating blood formed. Within the impingement region the AAA wall was devoid of ILT and remote to this region there was an accumulation of ILT. The high wall shear stress (WSS) caused by the impact of vortexes is thought to prevent the attachment of ILT. WSS from impingement is comparable to peak-systolic WSS in a normal-sized aorta and therefore may not damage the wall. Expansion occurred to a greater extent in the direction of jet impingement and the wall-normal force from the continuous impact of vortexes may contribute to expansion. It was shown that the impingement region has low oscillatory shear index (OSI) and recirculation zones can have either low or high OSI. No correlation could be identified between OSI and ILT deposition since different flow dynamics can have similar OSI values.

Keywords—Abdominal aortic aneurysm, Intraluminal thrombus, Pulsatile flow, Oscillating wall shear stress.

INTRODUCTION

An abdominal aortic aneurysm (AAA) is a dilatation of the aorta between the renal arteries and the iliac bifurcation. Dilatation weakens the aortic wall making it susceptible to rupture and currently the decision to repair an AAA is based on a diameter criterion of 5.5 cm in men and 5 cm in women. The risk of rupture is significant at sizes > 5.5 cm and increases with

diameter¹⁸; however, ruptured AAA (RAAA) can have diameters smaller than 5 cm, while others can reach sizes of 10–12 cm without rupture. The fact that rupture can occur at a wide range of sizes indicates additional criteria could be used to evaluate the susceptibility of AAA rupture.

The tangential force exerted on the arterial wall by blood flow, referred to as wall shear stress (WSS), is thought to be an important hemodynamic factor that regulates arterial health. Low WSS and oscillations in blood flow direction are dominant mechanisms that can lead to a deterioration of the arterial wall.³⁶ The fact that the majority of aortic aneurysms are infrarenal suggests hemodynamics specific to this region trigger the initial aortic dilation. Under resting conditions, only one third of the supraceliac flow rate is directed into the legs¹⁶ and WSS is substantially lower in the abdominal segment of the aorta.³⁵ Interestingly, it has been shown that patients with a single above-knee leg amputation are more likely to develop AAA.⁴⁰ In addition to further lowering WSS in the abdominal aorta, due to reduced blood requirement from the amputated leg, a single above-knee leg amputation causes an asymmetrical flow pattern at the aortic bifurcation. The majority of the blood flow being directed down a single iliac artery of the non-amputated leg causes a higher wall-normal pressure force to be applied along the side with the amputation and expansion was found to be more prevalent on this side.

It is common for intraluminal thrombus (ILT) to accumulate within AAA. Once a layer of ILT forms the aortic wall is no longer directly exposed to low and oscillating WSS and this can not be considered the cause of wall deterioration.¹⁷ The aortic wall receives oxygen primarily from luminal blood flow and a layer

Address correspondence to David C. S. Kuhn, Department of Mechanical Engineering, University of Manitoba, Winnipeg, MB, Canada. Electronic mail: david.kuhn@umanitoba.ca

of ILT may decrease the flow of oxygen (hypoxia), which in turn may decrease wall integrity, making it more susceptible to further expansion or rupture.⁴² It has been shown that ILT deposition increased AAA growth rate,^{25,44,48} and that regions of the AAA wall with ILT experienced localized hypoxia⁴¹ and were thinner with more inflammation.¹⁴ Alternatively it has been suggested that ILT is protective and shields the aortic wall from pressure forces.^{5,23,43,47} In Speelman *et al.*³² AAA wall stress was lower when a large ILT volume was present but growth rate was also higher. The authors stated that the deterioration of the aortic wall from ILT may be more significant than the hemodynamic forces acting on the wall. It has been suggested that ILT thickness could be used as a criterion, in addition to diameter, when determining risk of rupture³¹ and ILT deposition in small-sized AAA should be a factor when considering early surgical repair.^{33,44}

It is possible that zones of stagnant blood, turbulent fluctuations and flow impingement produce a hemodynamic environment that contributes to AAA expansion, ILT deposition and rupture. As an AAA increases in size adverse hemodynamic conditions may worsen, further increasing the risk of rupture. Since AAA can have a wide variety of shapes, it is possible that particular geometries have greater disturbances in blood flow. Some AAA may dilate to very large sizes while maintaining stable non-disturbed blood flow and therefore could potentially be at a lower risk for rupture. It would be beneficial to be able to identify the flow dynamics associated with particular aortic geometries.

In this current work we computationally investigated pulsatile blood flow dynamics in patient-specific AAA. The study consisted of 23 cases and we will be focusing our presentation on cases 1–4. The results indicate that the impingement of blood flow may prevent ILT deposition and influences the overall aneurysm shape. The remaining 19 cases will be referenced to further support this observation.

MATERIALS AND METHODS

Model Description

Case 1–3 have diameters of 6.8, 6.0 and 11 cm, respectively, and posterior-eccentric ILT of maximum thickness 1.8, 0.4 and 4.4 cm, respectively. For case 3 the ILT becomes circumferential-eccentric in the lower AAA segment. Case 4 has a diameter of 7.4 cm and is devoid of ILT. The models are generated from computed tomography angiography (CTA) images using the commercial medical imaging software Mimics-17.0 (Mimics, Materialise, Leuven, Belgium). To simplify

the geometry, arteries that branch off of the aorta, such as the visceral arteries, are excluded and the common iliac arteries are modeled to the bifurcation of the internal and external iliac arteries.

The non-dimensional parameters that govern blood flow are the bulk Reynolds number Re_b , Womersley number Wo and the oscillating-to-mean flow rate ratio β , which are, respectively,

$$Re_b = \bar{u}_b D_h / \nu, \quad (1)$$

$$Wo = D_h / 2 \sqrt{\omega / \nu}, \quad (2)$$

$$\beta = u_{osc} / \bar{u}_b. \quad (3)$$

Here $\nu = \mu / \rho$ is the kinematic viscosity, with μ and ρ being the dynamic viscosity and density, respectively, $\omega = 2\pi / T$ is the angular frequency, u_{osc} is the amplitude of the oscillating component of the pulse and \bar{u}_b is the time-average of the bulk velocity at the inlet boundary. The length scale used to define Re and Wo is the inlet hydraulic diameter $D_h = 4A / P$, where A and P are the cross-sectional area and perimeter of the upstream aorta inlet, respectively. Although blood is a non-Newtonian fluid it can be assumed to behave like a Newtonian fluid in large arteries.¹⁶ The governing equations for the conservation of mass and momentum, in a Cartesian coordinate system $\mathbf{x} = (x, y, z)$, are as follows:

$$\nabla \cdot \mathbf{u} = 0 \quad (4)$$

$$\partial \mathbf{u} / \partial t + \mathbf{u} \cdot \nabla \mathbf{u} = -\nabla p + \nu \nabla^2 \mathbf{u} \quad (5)$$

where the velocity field is given by $\mathbf{u} = (u, v, w)$, t is the time unit and $p = P / \rho$, with P being the pressure. Using physiologically-realistic flow conditions $\beta = 5.5$, $\mu = 0.0035 \text{ kg m}^{-1} \text{ s}^{-1}$, $\rho = 1050 \text{ kg m}^{-3}$ and $T = 1 \text{ s}$. The mean and maximum bulk flow rate is 20 and 130 ml s^{-1} , respectively. For the cases in this study, Re_b varied from 254–313 and Wo varied from 16.5–20.5. The x -axis is placed perpendicular with the axial plane and is referred to as the streamwise direction.

The temporal variation in the infrarenal bulk flow rate used in this study is shown in Fig. 1a. The term infrarenal refers to the segment of the aorta below the renal arteries. The pulse profile is from Les *et al.*,²⁰ where it was calculated from patients with AAA and the mean infrarenal flow rate was found to be $17.5 \pm 5.44 \text{ ml s}^{-1}$. The flow rate used in our study is then slightly above average for patients with AAA.

Systole refers to cardiac contraction and diastole to cardiac relaxation. At the end of systole, the infrarenal bulk flow rate reverses direction and throughout diastole the flow rate is effectively zero.

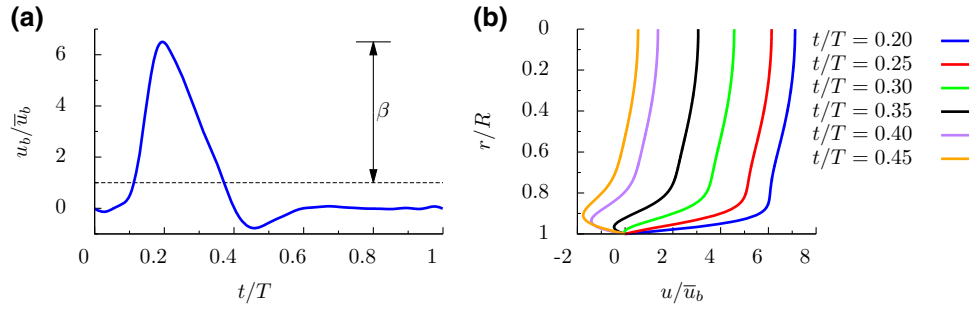


FIGURE 1. (a) Temporal variation in infrarenal bulk flow rate. (b) Analytical solution to a fully-developed pulsatile velocity profile in a pipe. Profiles calculated using bulk flow rate data from Les *et al.*²⁰

Simulation Details

The open source finite-volume code OpenFOAM-2.2.2 (OpenCFD Ltd, Bracknell, United Kingdom) is used to directly solve the governing equations. The code uses the PISO algorithm¹³ for pressure-velocity coupling, a second-order central difference scheme for the spatial derivatives and a second-order implicit Euler method for the time derivative. To satisfy a criterion of having the Courant-Friedrichs-Lewy (CFL) number < 1 the time-step is fixed at $\Delta t = 0.25 \times 10^{-5}$ s for case 1 and $\Delta t = 0.5 \times 10^{-5}$ s for cases 2–4. At each time-step the equations are considered converged when the residuals become less than 1×10^{-6} . The time-dependent bulk velocity from Fig. 1a is implemented at the upstream inlet boundary. A uniform velocity is used as the boundary condition, as opposed to a fully developed profile, since within the aorta only several cm are required for an oscillating boundary layer to develop⁴⁶ and at no point does the mean component reach a fully developed state.⁴ At the outlet boundaries, downstream in the iliac arteries, a reference pressure of $p = 0$ is imposed and the arterial walls are assumed to be rigid with a no-slip condition. The initial flow field is set to zero and statistics are collected after 5 pulses simulated to remove the effect of initial conditions. The time average of a flow quantity is represented by an overbar and is calculated by averaging over a period defined by $t_i = 5$ s and $t_f = 13$ s.

Unstructured grids composed of prism cells extruded from the wall and tetrahedral cells occupying the interior of the domain are generated using the commercial grid generation software Pointwise-17.2 (Fort Worth, Tex, US). The wall tangent edge length of the first prism cell adjacent to the wall is fixed at 0.002 cm and 15 prism cells are extruded at an expansion rate of 1.25. The edge length of the interior tetrahedral cells is fixed at 0.065 cm. The size of the grids used in this study varied from 6494498 to 13173579 and is comparable to those from previous studies.^{1,19,48} The grid resolution is assessed by comparing the average edge length of a grid cell Δ to the

time-averaged Kolmogorov length scale $\bar{\eta} = (v^3/\bar{\epsilon})^{1/4}$, where the term $\bar{\eta}$ gives the smallest scale of turbulent motion.²⁹ The term $\bar{\epsilon}$ is the time-averaged rate of turbulent kinetic energy (TKE) dissipation and is calculated using the triple decomposition method introduced by Hussain and Reynolds.¹² The instantaneous velocity field can be decomposed into

$$\mathbf{u} = \bar{\mathbf{u}} + \tilde{\mathbf{u}} + \mathbf{u}', \quad (6)$$

where $\bar{\mathbf{u}}$ is the time average, $\tilde{\mathbf{u}}$ is the periodic fluctuation, \mathbf{u}' is the turbulent fluctuation. Each period is segmented into $M = 50$ equidistant phase positions and at each phase $N = 25$ snapshots of the velocity field are collected. The average of \mathbf{u} locked at a phase is calculated as

$$\langle \mathbf{u} \rangle = \bar{\mathbf{u}} + \tilde{\mathbf{u}} = \frac{1}{N} \sum_{n=0}^{N-1} \mathbf{u}|_{t+nT} \quad (7)$$

and the turbulent fluctuation is $\mathbf{u}' = \mathbf{u} - \langle \mathbf{u} \rangle$. The instantaneous rate of TKE dissipation is calculated as $\epsilon = 2\nu \mathbf{s}' : \mathbf{s}'$, with $\mathbf{s}' = (\nabla \mathbf{u}' + \nabla \mathbf{u}'^T)/2$ being the fluctuating strain-rate tensor and the time-average of ϵ is calculated by averaging the 1250 instantaneous snapshots. This procedure has been performed for case 3 and the maximum $\Delta/\bar{\eta}$ is found to be 3.1 with a majority of the domain containing values < 2.5 . This indicates that the smaller turbulent fluctuations are sufficiently resolved by the grid.

Hemodynamics Analysis

Turbulent coherent structures are defined as spatial regions of high vorticity that maintain their shape for an extended period of time. Here they are visualized using the Q -criterion,¹¹ where Q is defined as $(\Omega^2 - \mathbf{S}^2)/2$, the tensors $\mathbf{S} = (\nabla \mathbf{u} + \nabla \mathbf{u}^T)/2$ and $\Omega = (\nabla \mathbf{u} - \nabla \mathbf{u}^T)/2$ are the strain and rotation-rate tensor, respectively. The quantity Q measures the amount the local vorticity magnitude exceeds the strain rate. The WSS vector $\boldsymbol{\tau}_w = (\tau_{w,x}, \tau_{w,y}, \tau_{w,z})$ is defined as

the tangential component of the surface traction vector $\mathbf{t} = \boldsymbol{\tau}\mathbf{n}_s$, where \mathbf{n}_s is a unit vector normal to the surface, $\boldsymbol{\tau} = 2\mu\mathbf{S}$ is the shear stress tensor. The tangential component of \mathbf{t} is isolated by subtracting out the normal component through

$$\boldsymbol{\tau}_w = \mathbf{t} - (\mathbf{t}\cdot\mathbf{n}_s)\mathbf{n}_s. \quad (8)$$

The time-averaged WSS (TAWSS) is a scalar defined as

$$\text{TAWSS} = \frac{1}{t_f - t_i} \int_{t_i}^{t_f} \|\boldsymbol{\tau}_w\| dt, \quad (9)$$

where $\|\cdot\|$ is the magnitude of a vector. The oscillatory shear index (OSI)¹⁰ quantifies the oscillation in the WSS vector's direction and is defined as

$$\text{OSI} = 0.5 \left(1 - \|\bar{\boldsymbol{\tau}}_w\| \text{TAWSS} \right). \quad (10)$$

Low OSI indicates a single dominate flow direction and high OSI indicates oscillations in the flow direction. The transverse time-averaged WSS (transWSS)²⁷ quantifies the disturbance in the WSS vector and is defined as

$$\text{transWSS} = \frac{1}{t_f - t_i} \int_{t_i}^{t_f} \left\| \boldsymbol{\tau}_w \cdot \left(\mathbf{n}_s \times \frac{\bar{\boldsymbol{\tau}}_w}{\|\bar{\boldsymbol{\tau}}_w\|} \right) \right\| dt. \quad (11)$$

Low transWSS indicates the WSS vector is predominately parallel with a single axis during the cardiac cycle and high transWSS indicates the WSS vector fluctuates about the dominate flow axis. Since a large range of TAWSS values can occur in AAA, transWSS was normalized by the local value of TAWSS.

RESULTS

Velocity Field

To better understand the expected flow dynamics in the abdominal aorta, the analytical solution to a fully-developed pulsatile velocity profile is calculated for a pipe segment of radius R , radial coordinate r , $Wo = 15$ and abdominal aortic flow conditions. The mean component of the analytical solution is a Poiseuille velocity profile and the oscillating component is calculated using Fourier coefficients obtained from the bulk flow rate data in Les *et al.*²⁰ The calculation of an oscillating velocity profile requires the bulk flow rate to be shifted to it's corresponding pressure gradient and this is done using correlations given by Womersley.⁴⁵ In Fig. 1b the analytical velocity profile is shown at various times during systole and early-diastole. As the blood flow decelerates, close to the wall it reverses in direction at $t/T = 0.29$. For all of diastole the velocity

profile consists of a low negative component close to the wall and a low positive component in the core region. Blood flow that oscillates in direction while maintaining a net positive direction is referred to flow reversal without separation.³⁷ Where as, blood flow with a flow direction at the wall that is opposite to the dominate direction is referred to as a recirculation zone.

The extent of the flow reversal that occurs for a given pulse profile is govern by Wo and this parameter defines the ratio of pulsatile inertia forces to viscous forces. Since ν and T are fixed parameters within the cardiovascular system, Wo is dependent on the size of the artery. In small arteries and capillaries, where $Wo \ll 1$, the pressure gradient is aligned with the flow rate and the flow can be treated as quasi-steady. As Wo is increased, the bulk flow rate begins to lag behind the pressure gradient.⁴⁵ Close to the arterial wall, oscillations in the blood flow will be more aligned with the oscillations in the pressure gradient compared to the blood flow in the center region of an artery. As described by Hale *et al.*,⁸ near wall velocity is low, therefore it will have less momentum and can be more easily reversed by the pressure gradient.

Figure 2 shows for case 1, mid-sagittal CTA, instantaneous and time-averaged contours of streamwise velocity plotted on the mid-sagittal section. During systole, the blood flow is predominately channeled within the AAA. By late-systole, a jet has formed that is directed towards the anterior wall and there is a small zone of recirculating blood along the posterior wall. During diastole, although the bulk flow rate in the abdominal aorta is effectively zero, the high momentum jet structures continue to flow downstream, shearing/impinging against the anterior wall and transition to turbulence. By $t/T = 0.56$ the structures have traversed to the mid-region of the AAA. In the upstream aorta, throughout the cardiac cycle, the blood flow behaves qualitatively similar to the analytical solution shown in Fig. 1b. The time-averaged streamwise velocity shows blood flow channeling along the anterior wall and a region of recirculating blood along the posterior wall. Referring to the mid-sagittal CTA, anterior wall is devoid of ILT and the posterior wall exposed to recirculation correlates with ILT deposition.

Figure 3 shows for cases 2–4, mid-sagittal CTA, instantaneous coherent structures visualized using the Q-criterion and time-averaged streamlines. During diastole for case 2 and 3, turbulent vortexes shearing along the anterior wall and recirculating blood occurs along the posterior wall. The wall is devoid of ILT at the impingement site and directly below this region ILT accumulates and the posterior wall has considerable ILT. White arrows shown on the CTA indicate

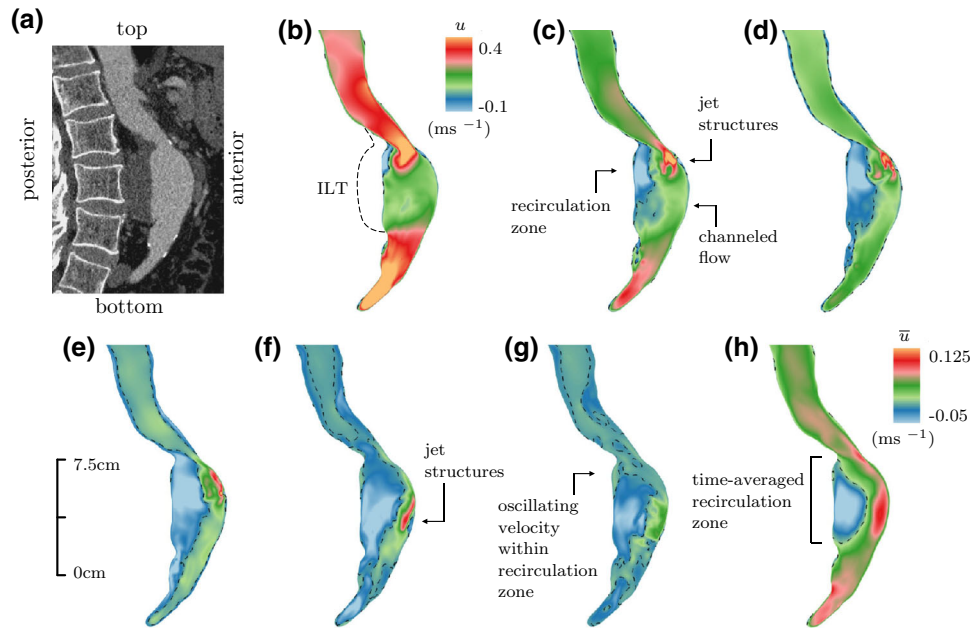


FIGURE 2. Case 1. (a) Mid-sagittal CTA. Instantaneous streamwise velocity at (b) $t/T = 0.24$, (c) $t/T = 0.32$, (d) $t/T = 0.36$, (e) $t/T = 0.4$, (f) $t/T = 0.56$ and (g) $t/T = 0.72$. (h) Time-averaged streamwise velocity. Dashed line in contours separates regions of positive and negative velocity. Dashed line outside flow channel in (b) shows ILT deposition.

the location on the anterior wall ILT starts to accumulate. Case 4 is devoid of ILT and although a jet forms at the neck during systole, the vortices stagnate at the neck region without propagating downstream into the AAA. The time-averaged streamlines indicate the blood flow is predominately channeled for this case.

Figure 4 and 5 shows for case 1 and 2, respectively, mid-axial CTA, instantaneous and time-averaged contours of streamwise velocity plotted on the mid-axial section. The jet is initially laminar and transitions to turbulence once it impacts against the wall. White arrows shown on the CTA indicate the location on the wall ILT starts to accumulate. The region of high velocity is devoid of ILT and the edge of this region correlates with the start of ILT accumulation. For case 1, the layer of posterior ILT results in the circular shaped AAA having an oval shaped lumen and the oval shape is tilted in the direction of impingement.

Wall Shear Stress

The peak WSS calculated from the analytical solution in Fig. 1b is 2.4 N m^{-2} and this value will be used as a reference. Figure 6 shows for case 1, anterior facing surface contours of $\tau_{w,x}$ at various times during diastole. From late-systole to early-systole of the next pulse the blood flow reverses in direction close to the wall and this results in the streamwise-component of WSS having low and negative values for a majority of

the cardiac cycle. Regions of elevated $\tau_{w,x}$ correspond to the impact of vortices against the wall. The peak WSS magnitude within the AAA occurs at $t/T = 0.52$ and is $\|\tau_w\| = 3.4 \text{ N m}^{-2}$. Although WSS caused by impingement is significantly higher than the surrounding regions in the AAA, it is comparable to the peak value obtained from the analytical solution. In the upstream aorta, peak WSS varies based on aortic diameter but is similar to the value predicted by the analytical solution.

Figure 7 shows for case 2, the streamwise-component of WSS plotted along the circumference of the axial slice shown in Fig. 5a. At peak-systole, $\tau_{w,x}$ is low and uniform along the circumference. During late-systole, $\tau_{w,x}$ continues to be low but has reversed in direction along the posterior-right side. During diastole, turbulent vortices shear pass the anterior-left side causing high and fluctuating WSS.

Surface contours of OSI for cases 1–4, are shown in Figs. 8a–8d. Since a uniform velocity was imposed at the inlet, OSI is low directly downstream of the inlet. Once an oscillating boundary layer develops, OSI is high within the straight segments of the aorta. For cases 1–3, the continuous blood motion from impingement causes low OSI within this region. Case 2's recirculation zone has low OSI, indicating continuous upstream motion caused by the jet's downstream motion on the opposite side. The recirculating zone for cases 2 and 3 contain regions with both high and low OSI values. High OSI within a recirculation zone is the

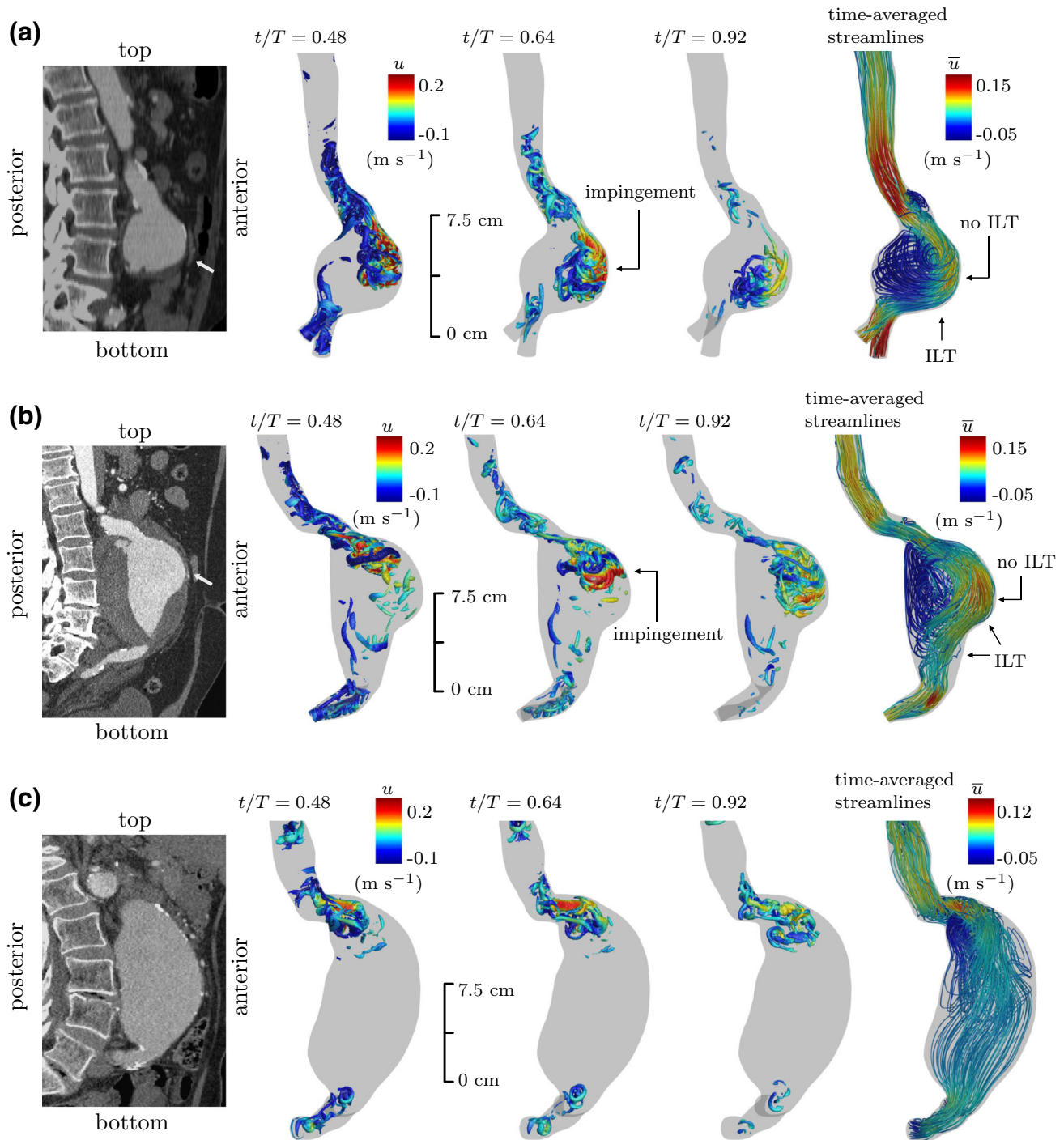


FIGURE 3. Mid-sagittal CTA with white arrow indicating the region on the anterior wall where ILT starts to accumulate, instantaneous coherent structures visualized using the Q-criterion and time-averaged streamlines for (a) case 2, (b) case 3 and (c) case 4.

result of oscillating velocity similar to that shown in Fig. 2d. For cases 2 and 3, directly below the impingement region OSI remains low and the lower anterior wall for case 3 has high OSI. For case 4, aside from the neck region, OSI is predominately high within the AAA.

Surface contours of normalized transWSS are shown for cases 3–4 in Figs. 8e and 8f. Within the straight segments of the aorta transWSS is low and this indicates that although the blood flow is highly oscillatory, the oscillations occur along a single axis. Within the impingement region, transWSS is high combined with

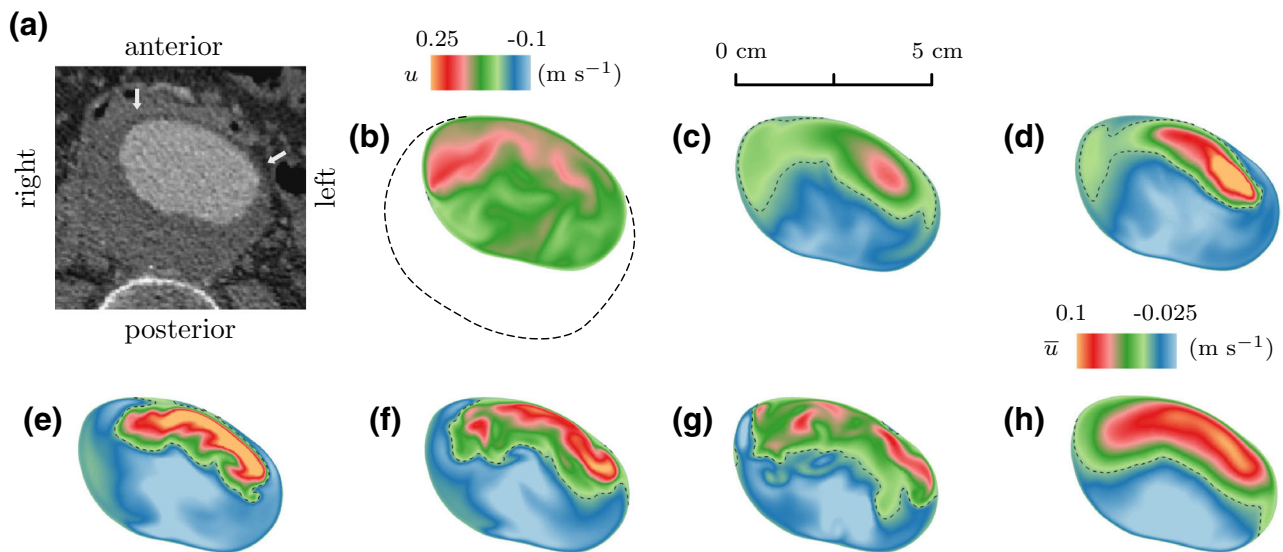


FIGURE 4. Case 1. (a) Mid-axial CTA with white arrows indicating the region on the aortic wall ILT starts to accumulate. Streamwise instantaneous velocity at (b) $t/T = 0.20$, (c) $t/T = 0.4$, (d) $t/T = 0.44$, (e) $t/T = 0.52$, (f) $t/T = 0.60$ and (g) $t/T = 0.72$. (h) Time-averaged streamwise velocity. Dashed line in contour separates regions of positive and negative velocity. Dashed line outside flow channel in (b) shows ILT deposition.

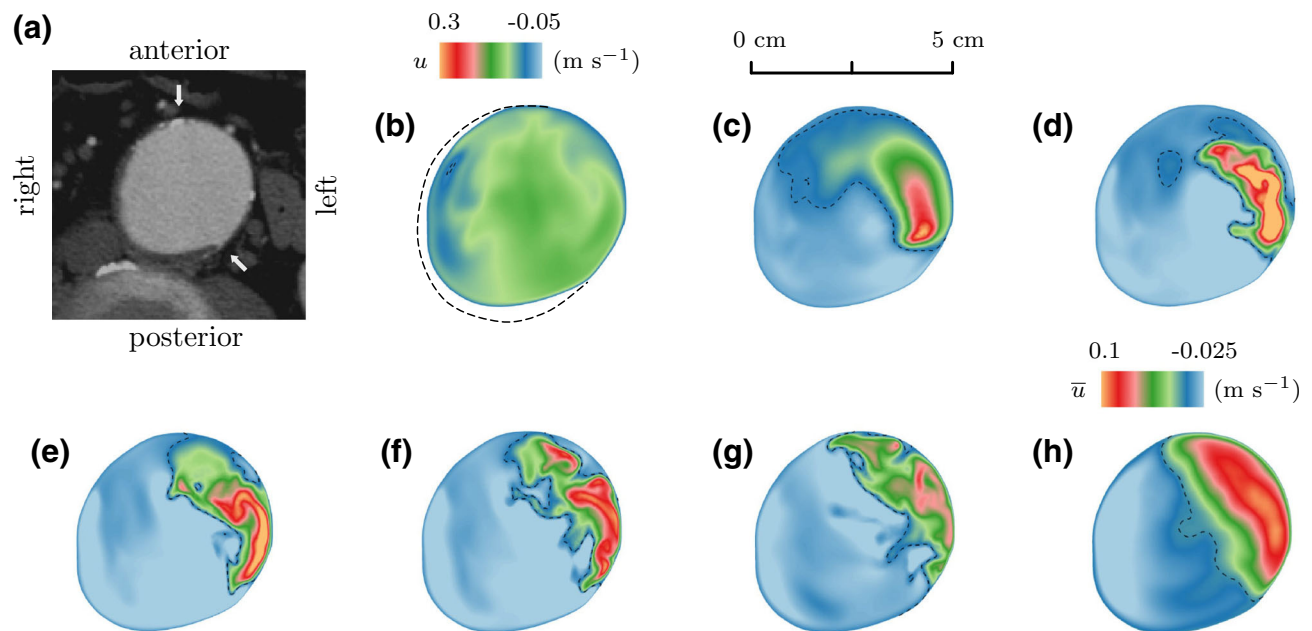


FIGURE 5. Case 2. (a) Mid-axial CTA with white arrows indicating the region on the arterial wall ILT starts to accumulate. Streamwise instantaneous velocity at (b) $t/T = 0.20$, (c) $t/T = 0.36$, (d) $t/T = 0.40$, (e) $t/T = 0.44$, (f) $t/T = 0.48$ and (g) $t/T = 0.56$. (h) Time-averaged streamwise velocity. Dashed line in contour separates regions of positive and negative velocity. Dashed line outside flow channel in (b) shows ILT deposition.

low OSI. This indicates the instantaneous WSS vector fluctuates about the dominate axis and the fluctuation remain directed along the dominate flow direction. Although case 4 has a large lumen, transWSS is predominately low, indicating laminar blood flow within the AAA. At most wall locations, an inverse relationship is found between OSI and transWSS.

DISCUSSION

Results are presented from simulations of pulsatile blood flow in four medium-to-large-sized AAA. It is found that a jet forms at the AAA neck during systole. For cases 1–3, during diastole turbulent vortexes from the jet continue to circulate within the AAA and im-

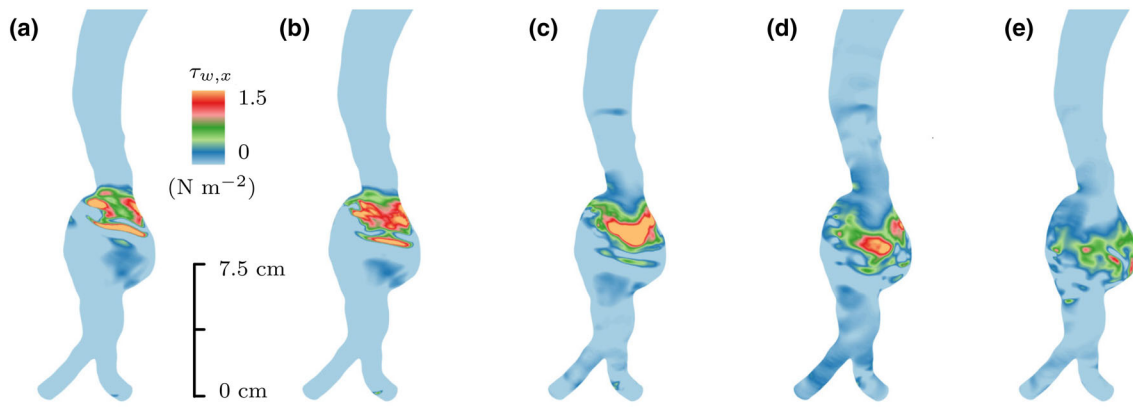


FIGURE 6. Case 1. Anterior facing surface contour of the instantaneous streamwise-component of WSS at (a) $t/T = 0.4$, (b) $t/T = 0.44$, (c) $t/T = 0.52$, (d) $t/T = 0.6$ and (e) $t/T = 0.72$. Light blue colour indicates $\tau_{w,x} \leq 0$.

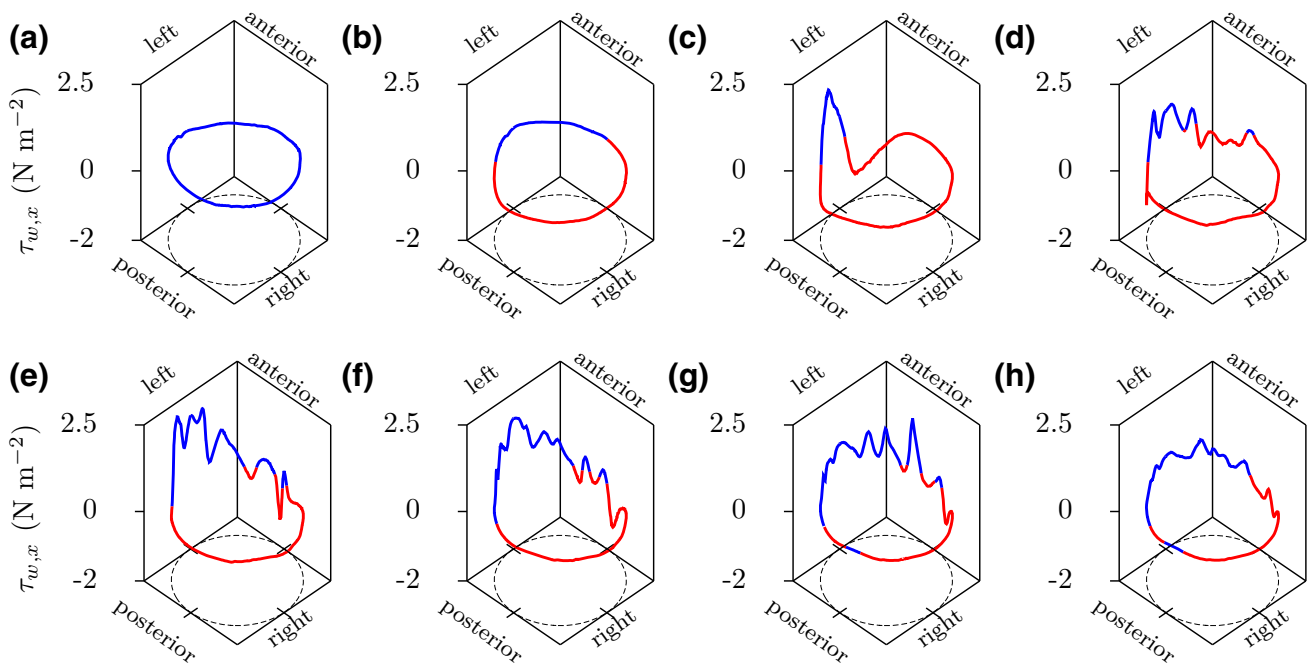


FIGURE 7. Case 2. Instantaneous streamwise-component of WSS plotted along the circumference of the mid-axial slice shown in Fig. 5a at (a) $t/T = 0.20$, (b) $t/T = 0.32$, (c) $t/T = 0.40$, (d) $t/T = 0.48$, (e) $t/T = 0.52$, (f) $t/T = 0.56$, (g) $t/T = 0.60$ and (h) $t/T = 0.64$. Blue and red color distinguishes positive and negative values, respectively.

pinge against the anterior wall with a zone of recirculating blood forming along the posterior wall. It can be seen in Figs. 3, 4, and 5 that the impingement site is devoid of ILT and there is a build-up in ILT remote from this region. Figure 7 shows that within the AAA, WSS caused by impingement is significantly higher than peak-systolic WSS. We present an argument that high WSS from the impact of a vortex prevents the attachment of ILT to the aortic wall.

It has been established by previous studies that recirculating blood correlates with vascular disease. Regions of recirculating blood have been shown to develop atherosclerosis in carotid bifurcation⁴⁹ and

ILT in intracranial aneurysms.³⁰ Doyle *et al.*⁷ investigated the growth and rupture in an AAA and it was shown that low WSS corresponded with the region with AAA growth, ILT deposition and rupture. Zambrano *et al.*⁴⁸ studied ILT growth in a group of 14 various sized AAA and observed ILT deposition occurred in regions with low WSS and ILT accumulation began in a localized region before spreading out to other regions. Since our present study uses a single static CTA for each case, it does not provided any new insight into the hemodynamic cause of ILT deposition. Rather it identifies a hemodynamic factor that may locally prevent the accumulation of ILT.

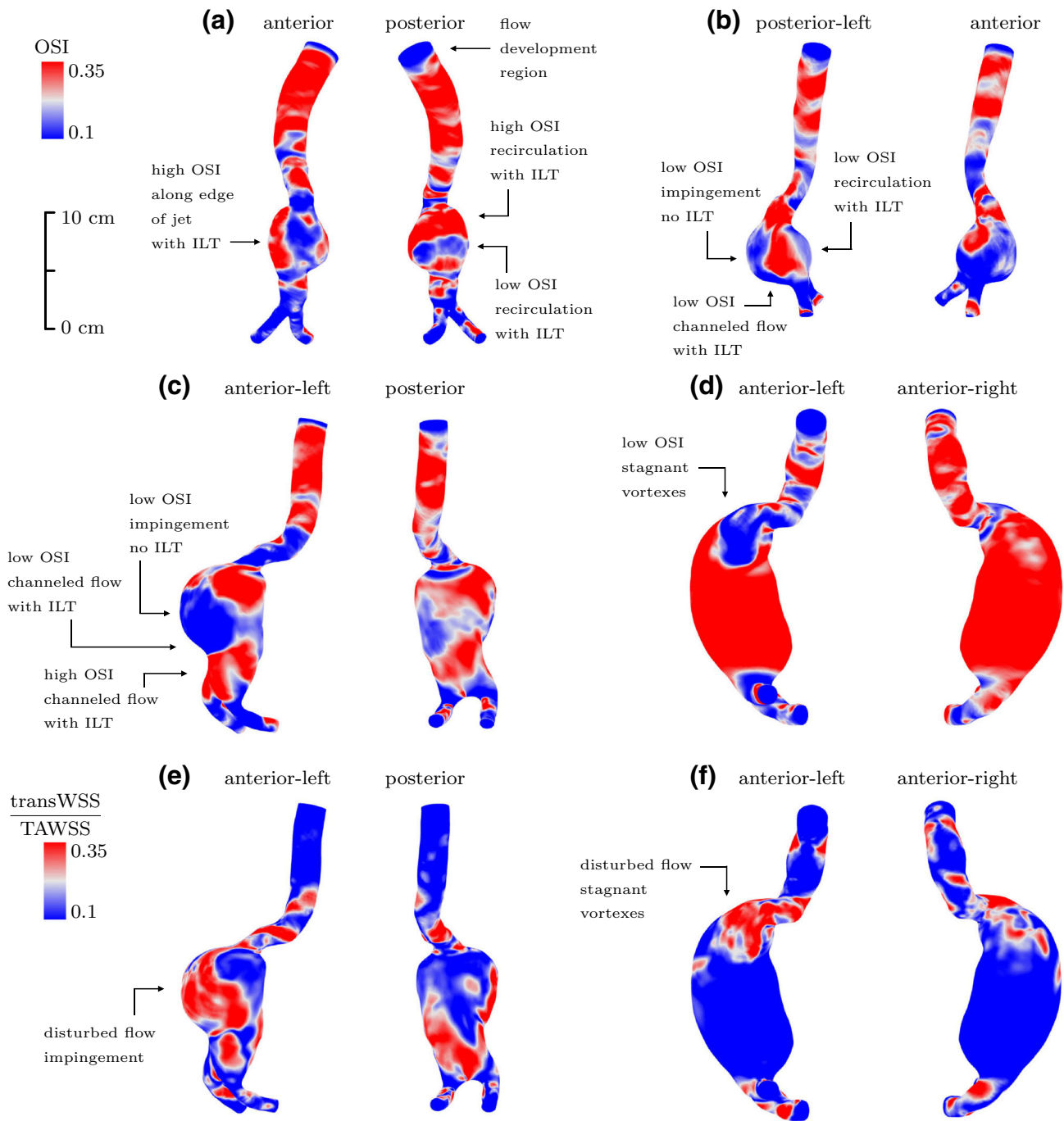


FIGURE 8. Surface contour of OSI for (a) case 1, (b) case 2, (c) case 3 and (d) case 4. Surface contour of normalized transWSS for (e) case 3 and (f) case 4.

It has been suggested high WSS from impingement in intracranial aneurysms contributes to growth and rupture²¹ and Dolan *et al.*⁶ defined high WSS as $> 3 \text{ N m}^{-2}$. Although our simulations showed WSS from impingement is relatively high, it is comparable to peak-systolic WSS in a straight normal-sized aorta. Therefore, vortices shearing along the wall may not directly damage the aorta. Caro *et al.*⁴ suggested

increased cardiac output from exercise would raise WSS and have a protective effect against atherogenesis. It has been shown exercise conditions raised WSS and lowered OSI within the abdominal aorta.^{35,38} Similar results were found to occur in AAA^{19,34} with it being suggested this would reduce AAA growth¹⁹ or the accumulation of ILT.⁴⁸ Exercise promoting aortic health by raising WSS is consistent with the concept of

high shear from impingement locally preventing ILT. An increased cardiac output is not considered a cardiovascular risk and this supports the hypothesis that impingement does not cause shearing damage.

It can be seen in Fig. 8 that cases 1–3 experience greater expansion on the side the flow structures impact. Although the continuous impact of these vortices may have a positive effect by locally preventing ILT, the wall-normal force exerted by these impacts could contribute to expansion. This is consistent with a previous finding that AAA from patients with single above-knee leg amputations were more likely to expand on the side with the amputation due to asymmetric blood flow⁴⁰ and it was suggested by Lasheras¹⁷ that tensional stresses, and not shear stresses, are the cause of AAA remodeling. Since impingement is found to occur primarily during diastole, the vortices are relatively slow-moving compared to peak-systole flow velocity. It can be speculated that although their impact may gradually influence expansion, it has insufficient force to be the cause of mechanical failure (rupture) in the wall. In our previous work, we examined the location of rupture in a group of 7 RAAA,³ and found that although high pressure and WSS occurred at the impingement site, rupture occurred in regions dominated by low WSS, recirculating blood and ILT deposition.

For this study a total of 23 AAA cases with diameter ≥ 5 cm were simulated. The AAA size, ILT location and impingement location if present, are summarized in Table 1. It is observed that blood flow

impingement similar to cases 1–3 only occurs in AAA with medium-to-large-sized lumen and requires a sudden expansion in lumen cross-sectional area at the neck. For AAA geometries with small-sized lumen or gradual increases in lumen diameter at the neck, flow structures stagnant at the neck (similar to what was seen with case 4). Irrespective of the size or shape of an AAA, during peak-systole the blood flow is channeled and predominately laminar. The time-averaged velocity field gives an overall description of the hemodynamics, but does not fully capture the disturbed flow dynamics that can occur during late-systole and diastole. For example, Fig. 2 shows the size of the recirculation zone varies with time and Fig. 6 shows the region of high WSS moves along with the vortices as they flow downstream.

Impingement is found to occur in 9 cases with the jet structures always flowing in the direction the neck angles the blood flow. For 8 of these cases, ILT of various thickness is present remote from the impingement site. Six cases have anterior-eccentric ILT and one case has circumferential-eccentric ILT. For these cases, a thick layer of ILT results in a small-sized lumen flow channel and the blood flow is stable without impingement or recirculation. From a single static CTA, it can not be identified what hemodynamic factors would cause ILT to deposit on the anterior wall. The remaining 7 cases experience flow dynamics similar to case 4, where there is no impingement and minimal ILT. Again this study does not identify why AAA similar to case 4 would develop.

TABLE 1. Patient information.

| Case | Sex | Maximum AAA diameter (cm) | Neck angulation (°) | Maximum ILT thickness (cm) | ILT deposition location | Impingement location |
|------|-----|---------------------------|---------------------|----------------------------|---------------------------|----------------------|
| 1 | M | 6.8 | 45 | 1.8 | Posterior | Anterior |
| 2 | M | 6.0 | 45 | 0.4 | Posterior-right | Anterior-left |
| 3 | M | 11.0 | 60 | 4.4 | Posterior | Anterior |
| 4 | M | 7.4 | 80 | 0.0 | – | – |
| 5 | F | 5.0 | 45 | 0.5 | Right | Anterior-left |
| 6 | M | 5.3 | 25 | 1.0 | Anterior | – |
| 7 | F | 5.5 | 60 | 1.0 | Circumferential-anterior | – |
| 8 | M | 5.5 | 40 | 1.4 | Posterior | Anterior |
| 9 | M | 8.0 | 45 | 2.8 | Circumferential-posterior | – |
| 10 | F | 5.4 | 70 | 0.0 | – | Left |
| 11 | M | 6.5 | 30 | 4.0 | Anterior | – |
| 12 | M | 5.5 | 20 | 2.0 | Right | Left |
| 13 | M | 6.9 | 35 | 2.8 | Anterior | – |
| 14 | M | 5.7 | 45 | 0.4 | Anterior-left | – |
| 15 | F | 6.6 | 0 | 2.0 | Circumferential-anterior | – |
| 16 | M | 5.5 | 0 | 1.0 | Posterior | – |
| 17 | M | 5.7 | 50 | 1.0 | Posterior | Anterior |
| 18 | M | 5.5 | 20 | 0.4 | Posterior-left-right | – |
| 19 | M | 5.9 | 15 | 1.0 | Circumferential | – |
| 20 | F | 5.5 | 20 | 2.4 | Anterior | – |
| 21 | M | 9.2 | 75 | 0.8 | Right | Left |
| 22 | M | 8.0 | 80 | 0.0 | – | – |
| 23 | M | 5.5 | 20 | 2.8 | Anterior | – |

Previous studies have shown it to be more common for ILT to be anterior-eccentric in AAA.^{9,22,28} Since our study showed impingement is primarily directed towards the anterior wall, this could indicate that the shape that leads to impingement is less common compared to other AAA shapes. In Metaxa *et al.*²² it was found that AAA with posterior-eccentric ILT have lower growth rates compared to AAA with anterior-eccentric ILT. Although impingement may contribute to expansion, the possible removal of ILT deposition along the anterior wall may result in a overall slower rate of growth compared to AAA with a thick layer of anterior-eccentric ILT. Despite case 4 having a large lumen, its blood flow is predominately non-disturbed and no ILT deposition was present. As such, it may represent a type of AAA geometry that is at lower risk of further growth and rupture.

The question was raised in Peiffer *et al.*²⁶ whether high OSI and low WSS adequately describe relevant blood flow features. Since WSS is proportional to diameter, in general WSS will decrease as AAA size increases. Although OSI provides a useful description of the flow dynamics, we believe within AAA it is not the correct metric to use when identifying abnormal hemodynamics. It should be noted that a wide variety of pulse profiles and values for Re_b and Wo can occur within the cardiovascular system. Any observations made for AAA hemodynamics may not hold for different cardiovascular locations. For example, typical non-dimensional parameters in intracranial aneurysms are $Re_b = 436$, $Wo = 1.8$ and $\beta = 0.6$ (Valen-Sendstad *et al.*³⁹). Although Re_b is similar between these cardiovascular locations the large differences in Wo and β will produce vastly different flow dynamics, i.e., in intracranial arteries high OSI may be an indication of disturbed flow behavior.²¹ Below is a summary of the observed flow dynamics compared with OSI and ILT deposition.

- At the location the jet structures impinge OSI is low, WSS and transWSS are high and the wall is devoid of ILT. Simply from this observation it could be concluded that low OSI has an preventative affect on ILT deposition; however, we believe that the mechanism is the shearing caused by the impact of vortexes and low OSI is only a consequence of this flow.
- For cases 2 and 3 directly below the impingement region OSI remains low and ILT accumulates. The blood flow in this region can be described as channeled and unidirectional.
- For case 3 along the lower segment of the anterior wall there is a thick layer of ILT and OSI is high. While case 4 has predominately high OSI and there is no ILT. This flow can be

described as a attached boundary layer that oscillates in direction. Figure 8a and 8b show that along the edge of the impingement region, blood flow exhibits this behavior and ILT is present.

- Zones of recirculating blood are characterized by low time-averaged velocity flowing opposite to the dominant flow direction. Figure 8a shows the recirculation zone can have distinct regions of both low and high OSI, and these variations do not appear to affect ILT thickness.

From this study a direct correlation can not be identified between OSI and ILT deposition or AAA shape. This is due to different flow dynamics having similar OSI values. Arzani *et al.*² performed a study on ILT growth in 10 small-sized AAA and regions with low OSI experienced the most ILT growth. Low OSI was thought to represent recirculating blood and this is consistent with what we observed in the recirculation zone of case 2. A similar observation was made by ORourke *et al.*²⁴ where, in three small-sized AAA, there was a correlation between regions with low OSI and ILT growth. Since both of these studies used small-sized AAA, they may have observed more normally channeled flow and not the greater disturbances in flow that can occur in larger AAA.

A limitation of this study is the model excluded arteries that branch off of the aorta and instead implemented the infrarenal flow rate at the supraceliac level in the aorta. Disturbances in the blood flow have been observed at the renal arteries.¹⁵ Since the bulk flow rate is effectively zero during diastole, these flow disturbances would stagnant at the renal arteries and not propagate downstream pass the AAA neck. Therefore it is unlikely that the inclusion of visceral arteries would significantly alter our results.

In conclusion, this study shows that high WSS from the impingement of vortexes is associated with an absence of ILT deposition. It is unlikely that impingement is beneficial, as the continuous impact of vortexes could, over an extended period of time, be contributing to AAA expansion. The continuous downstream motion from the vortexes results in low-velocity recirculation on the opposite side and this flow dynamic increases the likelihood of a layer of posterior-eccentric ILT forming. Wall hypoxia is potentially caused by the layer of ILT preventing adequate oxygen diffusion and this results in the deterioration of the posterior aortic wall; the typical location of aortic rupture.⁹ It would be beneficial to further investigate how the risk of rupture for an AAA with impingement and posterior-eccentric ILT compares to an AAA with stable blood flow and a layer of anterior-eccentric ILT.

ACKNOWLEDGMENTS

We acknowledge Grant support from the University Medical Group, Department of Surgery, University of Manitoba and computational resources provided by Western Canada Research Grid (WestGrid).

CONFLICT OF INTEREST

All authors declare that they have no conflict of interest.

STATEMENT OF HUMAN AND ANIMAL STUDIES

Ethics approval for this work was granted by the University of Manitoba Research Ethics Board, Research Protocol Number: REB B2013:130. No animal studies were carried out by the authors for this article.

REFERENCES

- ¹Arzani, A., A. S. Les, R. L. Dalman, and S. C. Shadden. Effect of exercise on patient specific abdominal aortic aneurysm flow topology and mixing. *Int. J. Numer. Methods Biomed. Eng.* 30(2):280–295, 2014.
- ²Arzani, A., G.-Y. Suh, R. L. Dalman, and S. C. Shadden. A longitudinal comparison of hemodynamics and intraluminal thrombus deposition in abdominal aortic aneurysms. *Am. J. Physiol. Heart Circ. Physiol.* 2014. DOI: [10.1152/ajpheart.00461.2014](https://doi.org/10.1152/ajpheart.00461.2014).
- ³Boyd A. J., Kuhn D. C., Lozowy R. J., and G. P. Kulbisky. Low wall shear stress predominates at sites of abdominal aortic aneurysm rupture. *J. Vasc. Surg.* 63(6):1613–1619, 2016.
- ⁴Caro, C. G., J. M. Fitz-Gerald, and R. C. Schroter. Atheroma and arterial wall shear observation, correlation and proposal of a shear dependent mass transfer mechanism for atherogenesis. *Proc. R. Soc. London. Ser. B Biol. Sci.* 177:109–133, 1971.
- ⁵Di Martino, E. S., S. Mantero, F. Inzoli, G. Melissano, D. Astore, R. Chiesa, and R. Fumero. Biomechanics of abdominal aortic aneurysm in the presence of endoluminal thrombus: experimental characterisation and structural static computational analysis. *Eur. J. Vasc. Endovasc. Surg.* 15:290–299, 1998.
- ⁶Dolan, J. M., J. Kolega, H. Meng. High wall shear stress and spatial gradients in vascular pathology: a review. *Ann. Biomed. Eng.* 41:1411–1427, 2012.
- ⁷Doyle, B. J., T. M. McGloughlin, E. G. Kavanagh, and P. R. Hoskins. From detection to rupture: a serial computational fluid dynamics case study of a rapidly expanding, patient-specific, ruptured abdominal aortic aneurysm. In: *Computational Biomechanics for Medicine*, edited by B. Doyle, K. Miller, A. Wittek, and P. M. F. Nielsen. New York: Springer, 2014, pp. 53–68.
- ⁸Hale, J. F., D. A. McDonald, and J. R. Womersley. Velocity profiles of oscillating arterial flow, with some calculations of viscous drag and the Reynolds number. *J. Physiol.* 128:629–640, 1955.
- ⁹Hans, S. S., O. Jareunpoon, M. Balasubramaniam, and G. B. Zelenock. Size and location of thrombus in intact and ruptured abdominal aortic aneurysms. *J. Vasc. Surg.* 41:584–588, 2005.
- ¹⁰He, X., and D. N. Ku. Pulsatile flow in the human left coronary artery bifurcation: average conditions. *J. Biomech. Eng.* 118:74–82, 1996.
- ¹¹Hunt, J. C. R., Wray, A. and P. Moin. Eddies, stream, and convergence zones in turbulent flows Center for Turbulence Research Report CTR-S88, 1988.
- ¹²Hussain, A. K. M. F., and W. C. Reynolds. The mechanics of an organized wave in turbulent shear flow. *J. Fluid Mech.* 41:241–258, 1970.
- ¹³Issa, R., I. Solution of the implicitly discretized fluid flow equation by operator-splitting. *J. Comput. Phys.* 62(1):40–65, 1985.
- ¹⁴Kazi, M., J. Thyberg, P. Religa, J. Roy, P. Eriksson, U. Hedin, and J. Swedenborg. Influence of intraluminal thrombus on structural and cellular composition of abdominal aortic aneurysm wall. *J. Vasc. Surg.* 38:1283–1292, 2003.
- ¹⁵Ku, D. N., S. Galgov, J. E. Moore, and C. K. Zarins. Flow patterns in the abdominal aorta. *J. Vasc. Surg.* 9:309–316, 1989.
- ¹⁶Ku, D. N. Blood flow in arteries. *Annu. Rev. Fluid Mech.* 29(1):399–434, 1997.
- ¹⁷Lasheras, J. C. The biomechanics of arterial aneurysms. *Annu. Rev. Fluid Mech.* 39:293–319, 2007.
- ¹⁸Lederle, F. A., G. R. Johnson, S. E. Wilson, D. J. Ballard, W. D. Jordan, Jr., J. Blebea, F. N. Littooy, J. A. Freischlag, D. Bandyk, J. H. Rapp, A. A. Salam, and I. Veterans Affairs Cooperative Study Rupture rate of large abdominal aortic aneurysms in patients refusing or unfit for elective repair. *JAMA* 287:2968–2972, 2002.
- ¹⁹Les, A. S., S. C. Shadden, C. A. Figueroa, J. M. Park, M. M. Tedesco, R. J. Herfkens, R. L. Dalman, and C. A. Taylor. Quantification of hemodynamics in abdominal aortic aneurysms during rest and exercise using magnetic resonance imaging and computational fluid dynamics. *Ann. Biomed. Eng.* 38:1288–1313, 2010.
- ²⁰Les, A. S., Yeung, J. J., Schultz, G. M., Herfkens, R. J., Dalman, R. L., and C. A. Taylor. Supraceliac and infrarenal aortic flow in patients with abdominal aortic aneurysms: mean flows, waveforms, and allometric scaling relationships. *Card. Eng. Tech.* 1:39–51, 2010.
- ²¹Meng, H., V. M. Tutino, J. Xiang, and A. Siddiqui. High WSS or Low WSS? Complex interactions of hemodynamics with intracranial aneurysm initiation, growth, and rupture: toward a unifying hypothesis. *Am. J. Neuroradiol.* 35:1254–1262, 2014.
- ²²Metaxa, E., N. Kontopodis, K. Tzirakis, C. V. Ioannou, and Y. Papaharilaou. Effect of intraluminal thrombus asymmetrical deposition on abdominal aortic aneurysm growth rate. *J. Endovasc. Ther.* 22(3):406–412, 2013.
- ²³Mower, W. R., W. J. Quiones, and S. S. Gambhir. Effect of intraluminal thrombus on abdominal aortic aneurysm wall stress. *J. Vasc. Surg.* 26:602–608, 1997.
- ²⁴O'Rourke, M. J., J. P. McCullough, and S. Kelly. An investigation of the relationship between hemodynamics and thrombus deposition within patient-specific models of abdominal aortic aneurysm. *Proc. Inst. Mech. Eng.* 226:548–564, 2012.

- ²⁵Parr, A., M. McCann, B. Bradshaw, A. Shahzad, P. Buttner, and J. Golledge. Thrombus volume is associated with cardiovascular events and aneurysm growth in patients who have abdominal aortic aneurysms. *J. Vasc. Surg.* 53:28–35, 2011.
- ²⁶Peiffer, V., S. J. Sherwin, and P. D. Weinberg. Does low and oscillatory wall shear stress correlate spatially with early atherosclerosis? A systematic review. *Cardiovasc. Res.* 99:242–250, 2013.
- ²⁷Peiffer, V., S. J. Sherwin, and P. D. Weinberg. Computation in the rabbit aorta of a new metric the transverse wall shear stress to quantify the multidirectional character of disturbed blood flow. *J. Biomech.* 46:2651–2658, 2013.
- ²⁸Pillari, G., J.B. Chang, J. Zito, J.R. Cohen, K. Gersten, A. Rizzo, et al. Computed tomography of abdominal aortic aneurysm. An in vivo pathological report with a note on dynamic predictors. *Arch. Surg.* 123:727–732, 1988.
- ²⁹Pope, S. B. *Turbulent Flows*. Cambridge: Cambridge University Press, 2000.
- ³⁰Rayz, V. L., L. Bousset, M. T. Lawton, G. Acevedo-Bolton, L. Ge, W. L. Young, R. T. Higashida, and D. Saloner. Numerical modeling of the flow in intracranial aneurysms: prediction of regions prone to thrombus formation. *Ann. Biomed. Eng.* 36:1793–1804, 2008.
- ³¹Satta, J., E. Laara, and T. Juvonen. Intraluminal thrombus predicts rupture of an abdominal aortic aneurysm. *J. Vasc. Surg.* 23:737–739, 1996.
- ³²Speelman, L., G. W. H. Schurink, E. M. H. Bosboom, J. Buth, M. Breeuwer, F. N. van de Vosse et al. The mechanical role of thrombus on the growth rate of an abdominal aortic aneurysm. *J. Vasc. Surg.* 51:19–26, 2010.
- ³³Stenbaek, J., B. Kalin, and J. Swedenborg. Growth of thrombus may be a better predictor of rupture than diameter in patients with abdominal aortic aneurysms. *Eur. J. Vasc. Endovasc. Surg.* 20:466–499, 2000.
- ³⁴Suh, G. Y., A. S. Tenforde, S. C. Shadden, R. L. Spilker, C. P. Cheng, R. J. Herfkens, R. L. Dalman, and C. A. Taylor. Hemodynamic changes in abdominal aortic aneurysms with increasing exercise intensity using MR exercise imaging and image-based computational fluid dynamics. *Ann. Biomed. Eng.* 39:2186–2202, 2011.
- ³⁵Tang, B. T., C. P. Cheng, M. T. Draney, N. M. Wilson, P. S. Tsao, R. J. Herfkens, and C. A. Taylor. Abdominal aortic hemodynamics in young healthy adults at rest and during lower limb exercise: quantification using image-based computer modeling. *Am. J. Physiol. Heart Circ. Physiol.* 291:H668–H676, 2006.
- ³⁶Tarbell, J. M., Z. Shi, J. Dunn, H. Jo. Fluid mechanics, arterial disease, and gene expression. *Annu. Rev. Fluid Mech.* 46:591–614, 2014.
- ³⁷Tardu, S. F., G. Binder, R. F. Blackwelder. Turbulent channel flow with large-amplitude velocity oscillations. *J. Fluid Mech.* 267:109–151, 1994.
- ³⁸Taylor, C. A., C. P. Cheng, L. A. Espinosa, B. T. Tang, D. Parker, and R. J. Herfkens. In vivo quantification of blood flow and wall shear stress in the human abdominal aorta during lower limb exercise. *Ann. Biomed. Eng.* 30:402–408, 2002.
- ³⁹Valen-Sendstad, K., K. Mardal, M. Mortensen, B. A. P. Reif, and H. P. Langtangen. Direct numerical simulation of transitional flow in a patient-specific intracranial aneurysm. *J. Biomech.* 44:2826–2832, 2011.
- ⁴⁰Vollmar, J. F., E. Paes, P. Pauschinger, E. Henze, and A. Friesch. Aortic aneurysms as late sequelae of above-knee amputation. *Lancet* 2:834–835, 1989.
- ⁴¹Vorp, D. A., P. C. Lee, D. H. Wang, M. S. Makaroun, E. M. Nemoto, S. Ogawa, and M. W. Webster. Association of intraluminal thrombus in abdominal aortic aneurysm with local hypoxia and wall weakening. *J. Vasc. Surg.* 34:291–299, 2001.
- ⁴²Vorp, D. A., W. J. Federspiel, and M. W. Webster. Does laminated intraluminal thrombus within abdominal aortic aneurysm cause anoxia of the aortic wall? *J. Vasc. Surg.* 23:540–541, 1996.
- ⁴³Wang, D. H., M. S. Makaroun, M. W. Webster, and D. A. Vorp. Effect of intraluminal thrombus on wall stress in patient-specific models of abdominal aortic aneurysm. *J. Vasc. Surg.* 36:598–604, 2002.
- ⁴⁴Wolf, Y.G., W. S. Thomas, F. J. Brennan, W. G. Goff, M. J. Sise, and E. F. Bernstein. Computed tomography scanning findings associated with rapid expansion of abdominal aortic aneurysms. *J. Vasc. Surg.* 20:529–535, 1994.
- ⁴⁵Womersley, J. R. Method for the calculation of velocity, rate of flow and viscous drag in arteries when the pressure gradient is known. *J. Physiol.* 127:553–563, 1955.
- ⁴⁶Wood, N.B. Aspects of fluid dynamics applied to the larger arteries. *J. Theor. Biol.* 199:137–161, 1999.
- ⁴⁷Xenos, M., N. Labropoulos, S. Rambhia, Y. Alemu, A. Tassiopoulos, N. Sakalihan, and D. Bluestein. Progression of abdominal aortic aneurysm towards rupture: refining clinical risk assessment using a fully coupled fluid structure interaction method. *Ann. Biomed. Eng.* 43:139–153, 2014.
- ⁴⁸Zambrano, B. A., H. Gharahi, C. Lim, F. A. Jaber, J. Choi, W. Lee and S. Baek. Association of intraluminal thrombus, hemodynamic forces, and abdominal aortic aneurysm expansion using longitudinal CT images. *Ann. Biomed. Eng.* 44:1502–1514, 2016.
- ⁴⁹Zarins, C. K., D. P. Giddens, B. K. Bharadvaj, V. S. Sotiurai, R. F. Mabon, and S. Glagov. Carotid bifurcation atherosclerosis. Quantitative correlation of plaque localization with flow velocity profiles and wall shear stress. *Circ. Res.* 53:502–514, 1983.